

Spatiotemporal genomic patterns of *Quercus gilva*: decoupling historical isolation from contemporary environmental adaptation

Shan-Shan Wang^{1,2#}, Tian-Rui Wang^{1#}, Ling-Ling Wang¹, Pei-Han Huang^{1,3}, Si-Di Liang¹, Si-Si Zheng¹, Liang-Hai Yang¹, Yu Li¹, Hong-Hu Meng³, Xin Zhong¹, Xiao-Chen Li¹, Bin-Jie Ge¹, Zi-Jia Lu¹, Yi-Xin Kang¹, Quan Yuan¹, Dong-Mei Jin¹, Xin Ning¹, Gregor Kozłowski^{1,4,5}, Young-Jong Jang⁶, Jin Xu^{2*}, Jung-Hyun Lee^{6*} and Yi-Gang Song^{1,7*}

¹ Key Laboratory of East China Plant Conservation and Utilization, National Forestry and Grassland Administration, Shanghai Chenshan Botanical Garden, Shanghai 201602, China

² School of Urban Construction and Ecological Technology, Shanghai Institute of Technology, Shanghai 201418, China

³ Plant Phylogenetics and Conservation Group, Centre for Integrative Conservation, Xishuangbanna Tropical Botanical Garden, Chinese Academy of Sciences, Kunming 650223, China

⁴ Department of Biology and Botanic Garden, University of Fribourg, Fribourg 1700, Switzerland

⁵ Natural History Museum Fribourg, Fribourg 1700, Switzerland

⁶ Department of Biology Education, Chonnam National University, Gwangju 61186, Republic of Korea

⁷ College of Forestry and Biotechnology, Zhejiang A & F University, Hangzhou 311300, China

Authors contributed equally: Shan-Shan Wang, Tian-Rui Wang

* Correspondence: xujin@sit.edu.cn (Xu J); quercus@chonnam.ac.kr (Lee JH); cherish-faith@163.com (Song YG)

Abstract

The interplay between historical biogeography and environmental selection shapes the genetic architecture of species; however, their relative contributions in widespread and ecologically important tree species remain poorly understood. In the Sino-Japanese Floristic Region, the East China Sea has alternately acted as a barrier and a corridor during glacial-interglacial cycles, influencing species isolation and contact. However, the extent to which these historical dynamics, along with environmental gradients, have driven adaptive evolution in dominant forest trees remains unresolved. In the present study, we integrated phylogeographic reconstruction and landscape genomics based on whole-genome resequencing data from 171 individuals across 35 populations to investigate the evolutionary history and adaptive mechanisms of *Quercus gilva*, a keystone evergreen oak, in East Asian subtropical forests. Population genomic analyses revealed two deeply divergent genetic groups: the China group and the Japan–Korea group, and demographic modeling indicated that their divergence dates back to the Miocene epoch. The relatively high genomic diversity of *Q. gilva* may result from the absence of severe genetic bottlenecks throughout its evolutionary history, multiple microrefugia during the glacial periods, and postglacial secondary contact. Notably, Quaternary glacial cycles repeatedly facilitated gene flow and admixture between these groups via exposed land bridges. Landscape genomic analyses further demonstrated that adaptive divergence in *Q. gilva* is shaped by both geographic isolation and environmental gradients, with annual precipitation emerging as the primary climatic driver. This study provides a genome-wide perspective on how historical biogeography and environmental selection interact to shape the genetic architecture of a dominant subtropical evergreen forest species, offering novel insights into the evolutionary dynamics and adaptive evolution across East Asian biodiversity hotspots.

Keywords: Climate change, East Asia, Evolutionary trajectory, Population structure, *Quercus gilva*, Whole-genome resequencing

Citation: Wang SS, Wang TR, Wang LL, Huang PH, Liang SD, et al. 2026. Spatiotemporal genomic patterns of *Quercus gilva*: decoupling historical isolation from contemporary environmental adaptation. *Forestry Research* 6: e016 <https://doi.org/10.48130/forres-0026-0016>

Introduction

Understanding evolutionary processes across spatiotemporal scales in a local context is critical for biodiversity conservation^[1,2]. Populations are the fundamental units of evolution and play a crucial role in maintaining the genetic diversity of species, environmental adaptation, and ecosystem restoration^[3]. To avoid local extinctions, populations must either track suitable habitats or adapt to new environmental conditions through the fixation of standing genetic variation and *de novo* mutations^[4–8]. Thus, dissecting evolutionary patterns through population genetics, demography, and geography helps us understand how genetic variation is distributed across landscapes and the evolutionary potential of species under future climate change^[9–12]. The recent development of high-throughput genomic tools has further enabled a shift from traditional phylogenetics and landscape genetics toward phylogenomics and landscape genomics.

Species have persisted through repeated periods of fluctuating climate, such as the Quaternary ice ages, which caused major

changes in global sea levels and the extent of continental ice sheets^[13]. Because of their sedentary lifestyle, long lifespans, and slow generation times, tree species often display geographic patterns of genetic variation largely shaped by local adaptation^[10–12]. East Asia remained largely ice-free during the ice ages, serving as a refugium for many woody plant taxa^[14–17]. The Sino-Japanese Floristic Region (SJFR), the core of East Asian subtropical evergreen broad-leaved forests (EBLFs), is a global hotspot of woody plant diversity with complex topography and relatively little impact from Quaternary glacial-interglacial cycles^[17–20].

Understanding the evolutionary history of EBLFs is essential not only for biodiversity conservation but also for predicting their responses to future climate change^[10–12,17,21–24]. Over the past two decades, phylogeographic studies using first-generation sequencing have examined various EBLF species^[19,20,25–29]. More recently, population genomic analyses using next-generation sequencing have provided deeper insights into the evolutionary history and adaptive mechanisms of these species^[10–12,23,24,30,31]. Collectively,

these studies reveal strong phylogeographic patterns shaped by monsoon evolution, Tibetan Plateau uplift, and geographic barriers^[19]. However, genomic insights into the evolutionary processes across spatiotemporal scales and the potential vulnerability of EBLFs under future climate change remain limited.

Quercus gilva is an endangered evergreen tree species with high ecological and cultural value^[32]. It occurs at low to middle altitudes, where it is heavily impacted by human activities. As a result, present-day populations of *Q. gilva* are mostly restricted to fengshui forests (e.g., around temples and shrines) and consist of only small numbers of individuals. Although widely distributed across the SJFR, its populations are sparse, small, and exhibit a scattered distribution^[32–34]. Recently, the genome of *Q. gilva* was published, facilitating studies on the ecological adaptation and evolution of oaks^[35]. Analyses of genetic diversity and population structure based on genome-wide variation have been conducted, but only on limited samples^[32]. Consequently, the roles of environmental and geographic gradients in shaping population differentiation, as well as the potential responses of *Q. gilva* to future climate change, remain poorly understood.

To address these gaps, we conducted a phylogeographic and landscape genomics study of *Q. gilva* using whole-genome resequencing data from the most comprehensively sampled natural populations of the species. Using genome-wide genetic variation, we inferred the spatial patterns of genetic diversity, population structure, and evolutionary trajectories of *Q. gilva*. We also quantified the contributions of environmental and geographic factors to these spatial genetic patterns. Finally, we evaluated the genomic vulnerability of different genetic groups under future climate scenarios. This study enhances our understanding of the spatiotemporal evolution of *Q. gilva* and informs conservation strategies for tree species in EBLFs under climate change.

Materials and methods

Sample collection and whole-genome resequencing

We sampled 171 individuals from 35 natural populations spanning the entire distribution range of *Q. gilva*, including populations from China, Japan, and South Korea (Supplementary Fig. S1, Supplementary Table S1). For each sample, genomic DNA was extracted from mature leaves using the standard cetyltrimethylammonium bromide (CTAB) method^[36]. DNA quality and concentration were assessed using 0.75% agarose gel electrophoresis, NanoDrop One spectrophotometer (Thermo Fisher Scientific), and Qubit 3.0 fluorometer (Life Technologies, Carlsbad, CA, USA). Sequencing libraries were constructed according to the manufacturer's instructions, followed by sequencing using combinatorial probe anchor synthesis (cPAS) technology^[37]. Paired-end sequencing (150 bp) was performed on a DNBSEQ-based platform (DNBSEQ-T7) using a commercial service (Wuhan Benagen Tech Solutions Company Limited, Wuhan, China).

Genome mapping and single-nucleotide polymorphism (SNP) calling

Adapter trimming and read filtering were performed using Fastp^[38] to obtain high-quality, clean paired-end reads. The specific steps included: removal of adapter sequences, trimming of trailing polyG/polyX sequences (minimum length: 10 bp), and discarding of reads containing more than 5 'N' bases, with an average quality score below 20, or more than 40% of bases having a quality score

below 15. Finally, reads shorter than 50 bp were excluded. The cleaned reads were aligned to the *Q. gilva* reference genome^[35] using BWA^[39] software with default parameters to generate the BAM files. The resulting files were sorted using SAMtools v1.9^[40] and duplicates were removed using Picard v2.18.11 (<http://broadinstitute.github.io/picard>). Genetic variant calling was performed using the Genome Analysis Toolkit (GATK v4.3.0.0) pipeline, employing the HaplotypeCaller, CombineGVCFs, and GenotypeGVCFs tools to generate a consolidated VCF file. After the initial variant calling, we used the GATK GenotypeGVCFs tool with the `-includeNonVariantSites` parameter to call variants and generate two datasets: one including 894,778,865 nonvariant sites, and the other containing 150,200,828 variant sites only. For the dataset that included nonvariant sites, filtering was performed using VCFtools v0.1.13^[41], retaining only biallelic sites with a minimum sequencing depth of 5 (`--minDP 5`) and a maximum missing rate of 20% (`--max-missing 0.8`). After filtering, 139,937,053 sites were retained for the estimation of nucleotide diversity (π) and for demographic history analyses. For the dataset excluding nonvariant sites, variant filtering was performed using the VariantFiltration tool with the following stringent criteria: `QD < 2.0 || FS > 60.0 || QUAL < 30.0 || SOR > 3.0 || MQ < 40.0 || MQRankSum < -12.5 || ReadPosRankSum < -8.0`, to filter the identified SNPs^[42]. Additional filtering was conducted using VCFtools v0.1.13^[41] with the following parameters^[11]: (1) `--minDP 5, --maxDP 50, --min-alleles 2, --max-alleles 2, --max-missing 0.8, --maf 0.05`, resulting in 17,396,250 SNPs (Dataset 1); (2) the same parameters applied to a dataset including five outgroups, resulting in 15,795,567 SNPs (Dataset 2); and (3) `--minDP 5, --maxDP 50, --min-alleles 2, --max-alleles 2, --max-missing 0.95, --maf 0.05`, resulting in 11,762,059 SNPs (Dataset 3).

Population structure and phylogenetic analysis

We performed linkage disequilibrium (LD) pruning on Datasets 1, 2, and 3 using PLINK v1.90^[43] with the following parameters: `-indep-pairwise 50 10 0.2`. Dataset 1 yielded 2,934,638 independent SNPs for population genomic analysis (including ADMIXTURE, principal component analysis [PCA], genetic diversity, differentiation, inbreeding, demographic history, and gene flow), and 1,026,841 independent SNPs were yielded from Dataset 3 for landscape genomic analysis (including Mantel tests, redundancy analysis [RDA], Gradient Forest [GF] analysis, BayeScan, latent factor mixed modelling [LFMM], and risk of non-adaptedness analysis [RONA])^[44]. Population structure analysis was inferred using ADMIXTURE v1.3.0^[45], with the number of ancestral clusters (K) tested from 1 to 10. The optimal K value was determined based on the lowest cross-validation error. To further explore the genetic relationships among individuals, PCA was conducted in PLINK^[46,47] using the LD-pruned SNP dataset. The resulting principal components (PCs) were visualized using the first two axes (PC1 and PC2) in R v4.2.2, implemented with the 'FactoMineR'^[48], 'factoextra'^[49], and 'ggplot2'^[50] packages.

Phylogenetic reconstruction based on Dataset 2 was performed using the Maximum Likelihood (ML) method in IQ-TREE v1.6.12^[51]. The SNP dataset was first converted from the VCF to the PHYLIP format (.phy) using the `vcf2phylip.py` script. The optimal nucleotide substitution model ("GTR + F + ASC + R6") was selected from 352 candidate models using ModelFinder^[52] under the Bayesian Information Criterion. Branch support was evaluated using 1,000 ultra-fast bootstrap replicates. The maximum likelihood tree was rooted using five outgroup species: *Quercus robur*, *Q. acutissima*, *Q. pachyloma*, *Q. augustinii*, and *Q. rex* (Data from unpublished work of our group). The final phylogenetic tree was visualized using FigTree v1.4.4 (<http://tree.bio.ed.ac.uk/software/figtree/>)^[53].

Divergence time estimation was conducted using Bayesian Markov Chain Monte Carlo (MCMC) algorithms implemented in BEAST v1.10. The best-fit substitution model ("GTR + F + ASC + R6") was selected using the ModelFinder^[52]. The Bayesian inference tree was calibrated using three fossil constraints derived from Fagaceae phylogeny: genus *Quercus* (60.52–55.18 Ma)^[54], section *Cyclobalanopsis* (48.98–47.70 Ma)^[55], and the divergence between *Q. jenseniana* and *Q. gilva* (24.80–17.87 Ma)^[54]. The MCMC chain was run with the following settings: a burn-in of 1,000,000 generations, sampling every 10 generations, and a total of 'pf' 500,000 samples. The final phylogenetic tree was visualized and edited using FigTree v1.4.4.

Genetic diversity, differentiation, and inbreeding analyses

To assess genome-wide patterns of genetic diversity and differentiation, we calculated π , inter-population divergence (D_{XY}), genetic differentiation (F_{ST}), and Tajima's D in 100-kb sliding windows using pixy v1.2.7^[56] for all loci (including non-polymorphic loci). To ensure robustness, stringent filtering was applied: genomic windows with effective site coverage (including both polymorphic and monomorphic sites) below 10% were excluded from π and D_{XY} calculations, and windows containing fewer than 20 SNPs were omitted from the F_{ST} estimation. We then used PopLDdecay v3.4.1 to calculate the LD decay within each group and compared the patterns between the two groups^[57].

Runs of homozygosity (ROH) were identified for each individual using PLINK v2.0^[46] with the following stringent parameters: --homozyg-kb 10, --homozyg-snp 50, --homozyg-density 50, --homozyg-window-snp 20, with ≤ 1 heterozygous and ≤ 5 missing calls, --homozyg-het 1, --homozyg-missing 5. The inbreeding coefficient (F_{ROH}) was calculated as the proportion of the genome contained within ROH regions, using the formula of $F_{ROH} = \frac{\sum L_{ROH}}{L_{auto}}$, where ' $\sum L_{ROH}$ ' represents the total length (in base pairs) of all ROH segments across the autosomes, and 'Lauto' represents the total physical length (in base pairs) of the autosomes covered by SNPs. Visualization of F_{ROH} distribution across individuals and populations was performed using the ggplot2 package in R.

Population history inference and gene flow analysis

Two coalescence-based methods were employed to reconstruct the population demographic history of *Q. gilva*. First, we inferred changes in the effective population size over time using SMC++ v1.15.4^[58], which employs a coalescent hidden Markov model. This method uses all genomic sites to estimate historical population size changes for the China and Japan–Korea groups. The results were scaled to real time using a generation time of 50 years, and a mutation rate of 1.01×10^{-8} per site per generation. To further validate the results and infer long-term population dynamics, we applied the Pairwise Sequentially Markovian Coalescent (PSMC) model using consensus sequences generated from the BAM alignment files of all individuals. The model was run with the parameter setting "4 + 25 * 2 + 4 + 6" and similarly scaled using the same generation time and mutation rate.

To investigate historical gene flow among the major genetic clusters, we used TreeMix v1.13^[59] to infer population splits and migration events. We tested models allowing between one and ten migration edges, calibrated on the maximum likelihood tree. To avoid overfitting, the -noss option was applied. To determine the optimal number of migration events, we used the OptM package in R for

model selection^[60]. For the selected optimal m value, we calculated the proportion of variance explained using the R script treemixVarianceExplained.R. The final tree was visualized in R. Additionally, to quantify introgression signals, we calculated the D-statistic (ABBA-BABA test) using Dsuite v0.3^[61]. We performed two separate analyses with the Dtrios function: one based solely on population assignments, and the other incorporating a known species tree to account for phylogenetic uncertainty. The results of both analyses were visualized as heat maps using the pheatmap package in R.

Correlation between genetic and environmental variation

We assessed the influence of spatial and environmental factors on the genetic differentiation in *Q. gilva* using Mantel tests and RDA. Pairwise F_{ST} values were calculated with VCFtools and transformed to genetic distances using the formula $F_{ST}/(1 - F_{ST})$ in the vegan R package^[62]. Nineteen bioclimatic variables were downloaded from WorldClim and filtered for multicollinearity ($|r| > 0.8$), using the usdm R package^[63]. Environmental and geographic distance matrices were generated using the stats and geosphere packages in R, respectively, and Mantel tests were performed with 9,999 permutations.

To further explore the environmental and spatial effects on genetic variation, we conducted RDA and partial RDA using the vegan package in R. SNP data were filtered and converted into individual-level allele frequency matrices, whereas the environmental predictors included six noncollinear bioclimatic variables and sampling coordinates. In partial RDA, geographic coordinates were treated as covariates to control for spatial autocorrelation. Model significance was evaluated via 999 permutations ($\alpha = 0.05$). We also applied gradientForest and extendedForest^[64,65] to characterize allele frequency turnover along environmental gradients and to identify key climatic drivers. Genetic input consisted of LFMM-format allele frequency data derived from filtered VCF files, and environmental input included sampling coordinates and six selected bioclimatic variables. GF analysis was performed using the R package with the following parameters: transform = NULL, compact = TRUE, nbin = 201, correlation threshold of 0.5 for predictor variables, and compact mode to optimize memory usage. The analysis assessed the contribution of each climatic variable to allelic variation, with results visualized using overall and cumulative importance plots.

Detection of selection signatures and adaptive loci

We investigated the genomic basis of climate adaptation using two complementary approaches: BayeScan^[66,67] for detecting loci under diversifying selection and LFMM^[68] to identify genotype–environment associations. For the BayeScan analysis, we converted the VCF files into the required format using the vcf2bayescan.pl script and ran the analysis with the following parameters: 20 pilot runs (5,000 iterations each), 50,000 burn-in steps, a thinning interval of 10, and a prior odds ratio of 100. Significant outlier loci were identified based on internally calculated q -values, which represent posterior probabilities corrected for the false discovery rate (FDR), using a threshold of $q < 0.05$. LFMM analysis was performed using the LEA package in R. Missing genotypes were first imputed via the 'snmf' function. Based on the inferred population structure ($K = 2$), 10 replicates of the LFMM model were run, each with 100,000 iterations and a burn-in of 50,000. To control for false positives due to multiple testing, we applied FDR correction, and SNPs with an adjusted p -value (q -value) < 0.05 were identified as significant

outliers associated with environmental variables. Functional annotation of all variant sites was performed using snpEff^[69], and Gene Ontology (GO) enrichment analysis was conducted with Annotation-Forge on two variant sets: (1) overlapping outliers identified by BayeScan and LFMM, and (2) missense variant SNPs.

Predicting future adaptive potential and ecological niche modeling

We used RONA to quantify theoretical allele frequency shifts and infer the adaptive potential of *Q. gilva* under future climate scenarios. Individual-level allele frequencies were extracted using the LEA package^[70] and regressed against six uncorrelated bioclimatic variables. The predicted allele frequencies for 2081–2100 under the SSP126 and SSP585 scenarios were generated using these models, and the average deviation from the present-day frequencies was calculated as the RONA value. Higher RONA values indicate greater genetic vulnerability and reduced adaptive potential.

Species distribution modeling was conducted in MAXENT v3.4.4^[71] using occurrence records and 2.5-arcmin resolution bioclimatic data from WorldClim across seven time periods: Last Interglacial (LIG), Last Glacial Maximum (LGM), Mid-Holocene, present (1970–2000), and three future windows under SSP126/SSP585. We screened the environmental variables for collinearity using the vifcor function (R package usdm) with a Pearson correlation threshold of $|r| > 0.8$. Following this screening, six predictors were retained for subsequent analyses: bio5 (maximum temperature of the warmest month), bio8 (mean temperature of the wettest quarter), bio9 (mean temperature of the driest quarter), bio12 (annual precipitation), bio15 (precipitation seasonality), and bio17 (precipitation of the driest quarter). Model tuning was performed using ENMeval, testing 48 combinations of regularization multipliers and feature classes. The optimal model ($\Delta AICc = 0$) was selected for final projections. Habitat suitability was classified in ArcGIS 10.2 based on logistic output into four categories: non-suitable ($p < 0.2$), low ($0.2 \leq p < 0.4$), moderate ($0.4 \leq p < 0.6$), and high suitability ($p \geq 0.6$), following thresholds previously applied in *Quercus* sect. *Heterobalanus*^[72]. The suitable area for each category was then quantified.

Results

Sequence data

We generated 2.999 Tb of clean sequencing data from 171 *Q. gilva* individuals (Supplementary Table S2). After quality filtering, three SNP datasets were obtained for downstream analyses: (1) Dataset 1: 2,934,638 SNPs for genetic structure analysis (filtered with --max-missing 0.8, retaining loci with $\leq 20\%$ missing data across samples). (2) Dataset 2: 2,763,859 SNPs, including five outgroups (*Q. acutissima*, *Q. pachyloma*, *Q. rex*, *Q. augustinii* and *Q. lobata*) for phylogenetic analysis. (3) Dataset 3: 1,026,841 SNPs for landscape genomic analysis (filtered with --max-missing 0.95, retaining loci with $\leq 5\%$ missing data across samples).

Population structure of *Q. gilva*

The ADMIXTURE analysis based on whole-genome resequencing data revealed two clearly differentiated groups within *Q. gilva*, with the lowest cross-validation error at $K = 2$ (Supplementary Fig. S2). These groups correspond to distinct geographic distributions: a China group and a Japan–Korea group (Fig. 1a, d). Similarly, PCA separated the 35 populations into two clusters, with PC1 and PC2

explaining 11.37% and 5.89% of the total variance, respectively (Fig. 1b). A ML phylogenetic tree constructed using IQ-TREE further supported the presence of two well-resolved clades corresponding to the two geographic groups (Fig. 1c).

Genetic diversity of *Q. gilva*

We quantified genome-wide genetic diversity of *Q. gilva* and genomic divergence between the China and Japan–Korea groups using pixy, revealing a heterogeneous landscape across chromosomes (π : 0.06×10^{-3} – 4.57×10^{-2} ; D_{XY} : 0.01862–0.1270; F_{ST} : 0.0007–0.2049; Fig. 2a, Supplementary Fig. S3). Notably, F_{ST} reached 0.2049 at specific loci, indicating moderate population differentiation. Nucleotide diversity (π) was marginally higher in the China group ($\pi = 1.41 \times 10^{-2}$) compared to that in the Japan–Korea group ($\pi = 1.39 \times 10^{-2}$), while overall genetic differentiation between the two groups was low ($F_{ST} = 0.028$, Fig. 2a, Supplementary Table S3). Tajima's D values were consistently negative across all chromosomes in both groups (mean: -1.1575 in China; -0.7052 in Japan–Korea), deviating significantly from expectations under neutral evolution (Fig. 2b, Supplementary Table S3). LD decay patterns differed between groups (Fig. 2c). The maximum r^2 values were 0.209 and 0.232 for the China and Japan–Korea groups, respectively. The corresponding LD decay distances (defined as the physical distance at which r^2 decreases to half of its maximum value) were estimated to be approximately 10 and 15 kb, respectively (Supplementary Table S4). The Japan–Korea group exhibited stronger LD and slower decay, suggesting a more constrained recombination landscape. The inbreeding coefficient (F_{ROH}) was calculated based on ROH longer than 10 kb across 171 individuals. ROH analysis revealed a slightly higher mean inbreeding coefficient in the Japan–Korea group compared with that in the China group (mean $F_{ROH} = 0.153$ and 0.144, respectively). In addition, the variation in the inbreeding coefficients among individuals was greater in the China group (standard deviations = 0.022 and 0.017, respectively) (Fig. 2d, Supplementary Table S5). The distribution of F_{ROH} values for all 35 analyzed populations is provided in the Appendix (Supplementary Fig. S4, Supplementary Table S5).

Divergence time, demographic history, and gene flow in *Q. gilva*

The Bayesian divergence time Inference tree based on 171 *Q. gilva* individuals and five outgroup taxa, inferred using MCMC methods, showed a topology consistent with ML results, resolving two major clades (Figs. 1c, 3). Divergence time estimates indicate an initial split within *Q. gilva* around 24.78 Ma (95% HPD: 23.73–25.80 Ma), followed by divergence of the China group at approximately 22.38 Ma (95% HPD: 21.17–23.50 Ma), and a subsequent split between the China and Japan–Korea groups at approximately 16.53 Ma (95% HPD: 15.38–17.66 Ma) (Fig. 3). Based on the SMC++ demographic reconstruction, there is no clear evidence of a population bottleneck for *Q. gilva*. The China group experienced an effective population size drop off between the Late Miocene and Early Pliocene (from 9 Ma to 4 Ma) and recovered afterwards, whereas the Japan–Korea group exhibited a similar shrink without recovery (Fig. 4a). PSMC analyses showed synchronized expansion and contraction phases of both groups (Fig. 4b).

By integrating TreeMix and Dsuite analyses, this study systematically revealed complex historical gene flow patterns among populations. Based on model selection using the OptM package in R (Supplementary Fig. S5), an optimal TreeMix model ($m = 8$) was selected. This model identified multiple significant gene flow events, including the migration from JWK to ZZS (weight = 0.0360) (Fig. 4c,

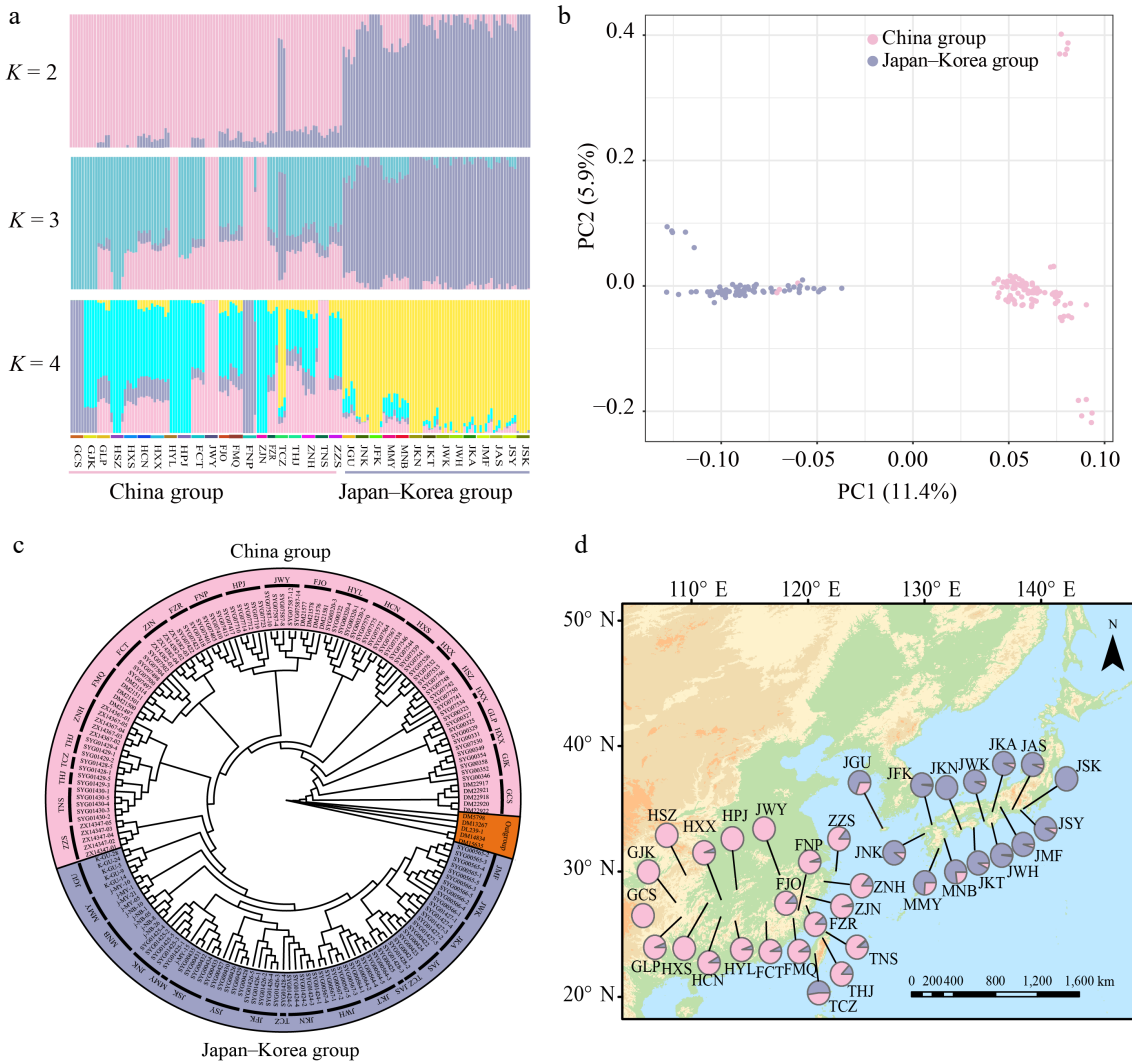


Fig. 1 Geographic distribution and population genetic structure of *Quercus gilva*. (a) ADMIXTURE bar plots for $K = 2$, $K = 3$, and $K = 4$. The x-axis represents populations, and the y-axis shows the inferred ancestry proportions. (b) Principal component analysis (PCA) with color-coding to indicate different groups of *Q. gilva*. Light pink and lavender-blue represent clusters in China, and Japan–Korea, respectively. (c) Maximum likelihood (ML) phylogenetic tree of 171 *Q. gilva* individuals and five outgroup taxa. (d) Geographical distribution of the 35 sampled populations with color-coded groupings based on the structure analysis ($K = 2$).

Supplementary Tables S6, S7). Dsuite analyses further supported widespread introgression: ZZS exchanged alleles with multiple Japanese populations, whereas GCS showed signals of introgression with all taxa except GJK. Additionally, significant gene flow was observed between TCZ and ZZS/MNB, THJ and ZZS/MNB/ZNH/FMQ, and TNS and ZNH/ZJN/FMQ (Fig. 4d, Supplementary Table S8). In summary, the optimal TreeMix model and D-statistics analyses revealed bidirectional but asymmetric gene flow between the China and Japan–Korea groups. These results not only confirm the historical genetic contributions of the China group to surrounding regions but also reveal reverse gene flow from the Japan–Korea group to the China group, reflecting the complex genetic exchange network in East Asia.

Landscape genomic characteristics of *Q. gilva* and their vulnerability responses to future climate change

The Mantel test revealed a significant correlation between genetic and geographic distances (isolation by distance (IBD): $r = 0.188$, $p = 0.003$) (Fig. 5a), but no significant correlation was observed

between genetic and environmental distances (isolation by environment (IBE): $r = -0.181$, $p = 0.89$) (Fig. 5b). Several climatic variables showed significant correlations with genetic variation, including mean temperature of the wettest quarter (bio8), mean temperature of the driest quarter (bio9), annual precipitation (bio12), and precipitation seasonality (bio15) (Mantel's $r = -0.092$, $p = 0.024$; Mantel's $r = -0.213$, $p < 0.001$; Mantel's $r = -0.118$, $p = 0.004$; Mantel's $r = -0.148$, $p < 0.001$, respectively) (Supplementary Fig. S6). RDA indicated that genetic variation was significantly associated with bio5, bio8, bio9, bio12, and bio15, of which bio9 and bio15 showing the strongest effects (Proportion of Variance Explained (PVE) = 0.0093, $p = 0.001$) (Fig. 5c, Supplementary Table S9). We further assessed the proportion of genetic variation explained by environmental factors and geographic variables using partial redundancy analysis (pRDA) to infer the primary drivers of genetic diversity (Table 1). pRDA revealed that environmental factors (4.73%) had a significantly stronger explanatory power than that of geographic factors (1.95%). Even after controlling for geographic variables, the independent contribution of environmental factors remained substantial (4.33%), whereas that of the geographic factors was

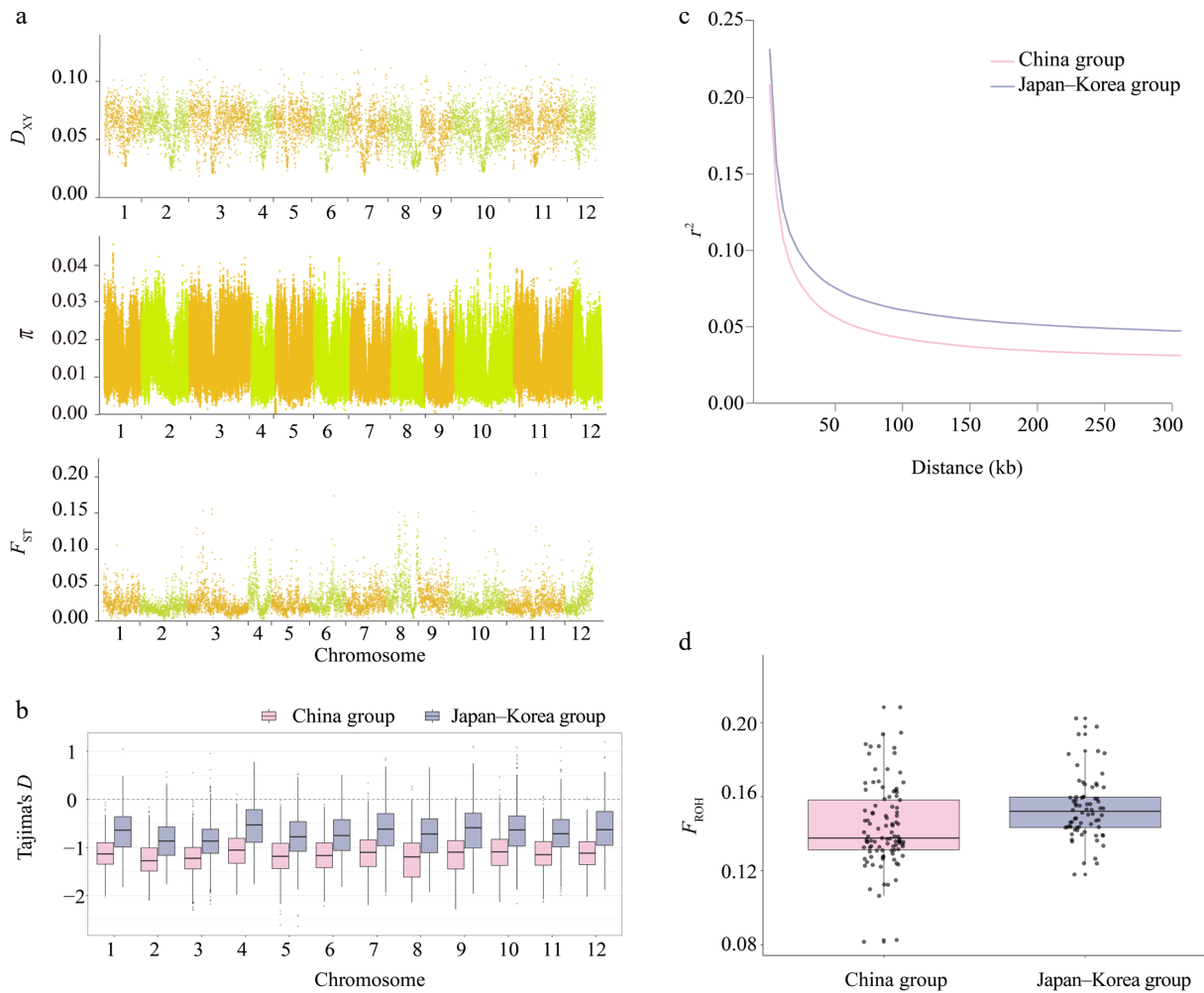


Fig. 2 Heterogeneity in genomic diversity and genomic divergence between the China and Japan-Korea groups of *Q. gilva*. (a) Manhattan plot showing the distribution of D_{XY} , π , and F_{ST} values between the two populations across chromosomes 1–12. The x-axis indicates the chromosomal position (cumulative physical position), and the y-axis indicates the values of D_{XY} , π , and F_{ST} . Each data point corresponds to a 100-kb sliding window. Chromosomes are alternately colored in light orange and light green to distinguish chromosome boundaries. (b) Comparison of Tajima's D across autosomes between two East Asian clusters. Boxplots show the distribution of Tajima's D values on chromosomes 1–12 for the China group (light pink) and the Japan-Korea group (lavender blue). (c) Linkage disequilibrium (LD) decay patterns in the two groups. (d) Comparison of inbreeding coefficients (F_{ROH}) between two populations of *Q. gilva*. Light pink and lavender blue represent the China group and the Japan-Korea group, respectively.

relatively weak (1.55%). This suggests that environmental filtering (e.g., climate) plays a dominant role in shaping genetic structure, whereas geographic factors (e.g., spatial distance) have a minor influence or are partially dependent on environmental variation. The full model explained only 6.28% of the total genetic variation, indicating that unmeasured factors (e.g., biotic interactions or stochastic processes) could also significantly influence the population genetic structure (Table 1).

The GF analysis identified geography as the primary driver of genetic variation in *Q. gilva*, followed by annual precipitation (bio12). Among the climatic variables, bio12, precipitation of the driest quarter (bio17), and precipitation seasonality (bio15) consistently ranked highest in importance across the r^2 -weighted and cumulative importance metrics. I-spline plots were generated for the top six predictors based on r^2 -weighted importance (Fig. 5d, e, Supplementary Fig. S7), which confirms the dominant role of these precipitation-related variables. These results highlighted the key roles of spatial structure and precipitation in shaping genetic patterns.

We assessed the genomic vulnerability of *Q. gilva* populations under future climate projections (SSP126 and SSP585, year 2081–2100) using RONA. The overall vulnerability of *Q. gilva* was higher

under SSP585 (Fig. 5g, Supplementary Table S10) than under SSP126 (Fig. 5f, Supplementary Table S10). Quantification of the genetic offsets identified three climatic variables as the key drivers: annual precipitation (bio12), maximum temperature of the warmest month (bio5), and mean temperature of the driest quarter (bio9). Among these, bio12 consistently influenced the adaptive potential across all populations.

Ecological niche modeling

Ecological niche modeling using MaxEnt (optimal parameters: RM = 2.5, FC = LQ) achieved high predictive accuracy (area under the curve (AUC) > 0.95; Supplementary Fig. S8, Supplementary Table S11). Projections across seven time periods revealed a dynamic distributional history. During the LGM, the exposure of land bridges facilitated an expansion of suitable habitat, which subsequently contracted during the Mid-Holocene, together displaying a unimodal trend (Fig. 6, Supplementary Table S12). Both the high- and medium-suitability areas exhibited similar temporal patterns. Future projections under SSP126 and SSP585 indicate continued range expansion, with high-suitability areas generally increasing,

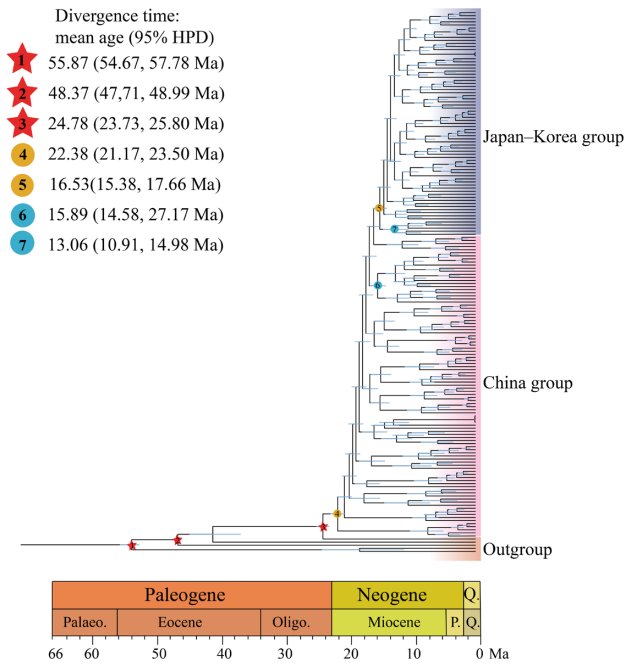


Fig. 3 Divergence times estimated using BEAST, with blue bars indicating 95% highest posterior density (HPD) intervals. Note that red five-pointed stars indicate the three selected fossil calibrations. Geological time abbreviation: P. = Pliocene; Q. = Quaternary. Circles represent divergence time estimates for *Q. gilva* populations: (4) divergence of *Q. gilva* populations in China; (5) divergence between the China and Japan–Korea groups; (6) divergence between the Zhejiang and Taiwan populations; (7) divergence between Japanese and Korean populations.

except for a slight decline during 2041–2060 under SSP126. Presently, suitable habitats are concentrated in subtropical East Asia, including eastern Guizhou, Hunan, Jiangxi, Fujian, Zhejiang, Taiwan, Jeju Island, and parts of Japan, which are characterized by monsoonal climates. During the LGM, the habitat contracted southward owing to glaciation, but refugia remained in the Nanling and Wuyi Mountains, Taiwan, and southern Japan. In contrast, the Mid-Holocene was characterized by northward range expansion, most notably in Japan. Under future scenarios, *Q. gilva* is predicted to expand its range, particularly into mountainous and monsoonal regions (Fig. 6, Supplementary Fig. S9).

Adaptive potential of *Q. gilva*

To identify the potential genetic loci underlying local adaptation between the two *Q. gilva* populations, we performed a genome-wide F_{ST} analysis. The Manhattan plot (Fig. 7a) revealed a heterogeneous distribution of F_{ST} values across the genome with prominent peaks on chromosomes 8 and 10, indicating strong population differentiation in these regions. We acknowledge that elevated F_{ST} values can arise from various factors, such as demographic history or genetic drift.

To more directly infer the role of natural selection, we employed two complementary genome-wide scanning approaches using the original genotype data, independent of the initial F_{ST} analysis: outlier detection using BayeScan to identify SNPs with allele frequency differentiation significantly exceeding neutral expectations, and environmental association analysis using LFMM to detect SNPs whose allele frequencies correlate with key climatic variables.

BayeScan identified 113,552 outlier SNPs (Supplementary Fig. S10), whereas the LFMM detected 311,414 SNPs associated with the six climatic variables (Supplementary Fig. S11). Integrative analysis

revealed extensive overlap between these two sets of candidate signals across the significance thresholds. For example, at $p \leq 0.05$, there were 277,539 environment-associated SNPs, 79,677 outlier SNPs, and 33,875 shared loci (Supplementary Fig. S12). A similar pattern was observed under more stringent thresholds: at $p \leq 0.01$, there were 138,712 environment-associated SNPs, 97,171 outlier SNPs, and 16,381 shared loci (Fig. 7b).

The set of loci identified by both methods (e.g., the 16,381 shared SNPs at $p \leq 0.01$) exhibit divergence that is both exceptional (outlier status) and environmentally correlated, making them high-confidence candidates for local adaptation. Based on this high-confidence candidate set ($p \leq 0.01$, specifically the 16,381 shared loci), we performed GO enrichment analysis. The results showed that these candidate loci were significantly enriched in the core biological processes of *Q. gilva*, including disease resistance defense (e.g., salicylic acid/jasmonic acid metabolism), growth and development regulation (e.g., flowering and root system establishment), stress response (e.g., reactive oxygen species metabolism), and fundamental molecular processes (e.g., protein modification and nucleocytoplasmic transport) (Supplementary Table S13).

Functional annotation of *Q. gilva* identified four mutation types, with missense mutations being the most frequent, followed by loss-of-function, nonsense, and synonymous mutations (Fig. 7c). GO enrichment analysis of the missense mutation sites revealed their predominant involvement in plant metabolic regulation, transcriptional control, protein modification, and enzymatic activities (Fig. 7d, Supplementary Table S14).

Discussion

The evolution of a taxon across vast spatial and temporal scales provides a unique opportunity to investigate its environmental adaptations and to address challenges posed by climate change. Population genomics has enabled a deeper understanding of the factors shaping genetic variation within and between populations under an 'Isolation-Connection-Isolation' dynamic in a well-delimited biogeographic region^[17,19,26–29]. Landscape genomics offers insights into the genomic mechanisms underlying local adaptation and allows quantification of populations' potential maladaptation to future climate change^[5,6,73]. Therefore, our study aimed to contextualize genome-wide genetic variation in *Q. gilva* within the framework of geography and climate change in the SJFR of the EBLFs.

Using 35 natural populations spanning the entire distribution range of *Q. gilva*, we demonstrate that this species exhibits a consistent biogeographic break across the East China Sea (ECS), corresponding to the phylogeographic differentiation between the China and Japan–Korea groups^[17,19,20,23–27]. Although this pattern has been identified in several taxa using first- and second-generation sequencing data, substantial discrepancies persist in the estimated divergence times^[19,74]. Both geographic and environmental gradients jointly shaped the differentiation of *Q. gilva* into these two groups. Molecular evidence strongly supports the environmental adaptation hypothesis of this species, indicating that precipitation exerts a significantly stronger selective pressure than temperature.

Geographical origin, divergence, and demographic history of *Q. gilva* Miocene origin and eastward expansion

East Asian subtropical EBLFs developed concomitantly with Asian monsoon systems and occurred no earlier than the Eocene^[17,75,76].

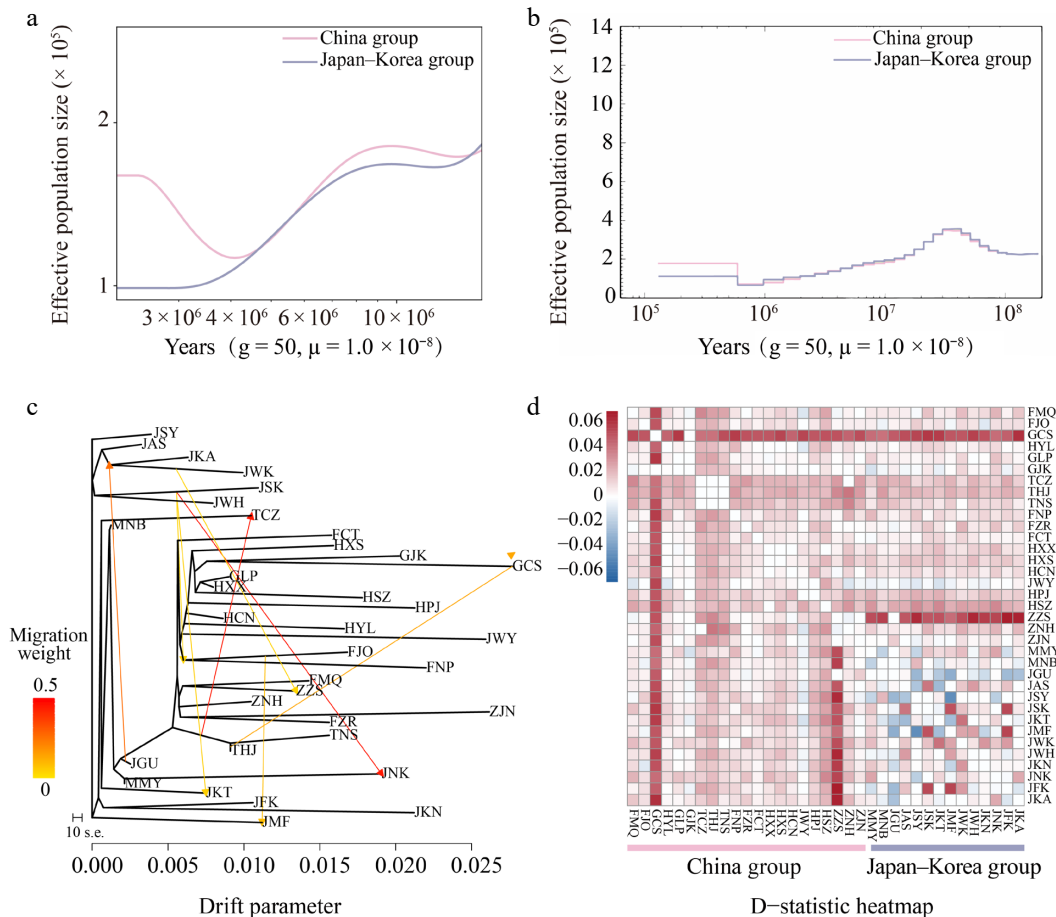


Fig. 4 Inferred demographic histories of the China (light pink) and Japan–Korea groups (lavender-blue) based on (a) SMC++, and (b) PSMC analyses. (c) Maximum likelihood (ML) tree constructed with TreeMix, allowing for eight migration events. Migration arrows are color-scaled by weight. (d) Introgression analysis with Dsuite was presented as a heatmap, where darker shades indicate higher introgression proportions between populations. For each trio (P1, P2, P3), the D value was mapped to P2 vs. P3 as positive (+D) and to P1 vs. P3 as negative (–D).

The current EBLFs harbor an unique assemblage comprising boreotropical relicts, tropical flora, and deciduous broad-leaved forests^[17,19,20,23–27,32,77]. Our study suggests that *Q. gilva* initially diversified in southwestern China, followed by eastward dispersal to eastern China and Japan, driven by an enhanced East Asian monsoon during the Early to Middle Miocene. We also dated the divergence between the China and Japan–Korea groups between the late Early Miocene and the Early Mid-Miocene. The Japanese archipelago began to separate from the Eurasian continent approximately 24 Ma^[19]. This indicates that a corridor across the ECS existed for species dispersal between East Asia and Japan during the early Mid-Miocene. Our newly estimated divergence time for this differentiation coincides with increasingly colder and arid climates following the Mid-Miocene Climatic Optimum (ca. 17–15 Ma)^[78,79]. Consistent with previous studies, *Q. gilva* dispersed eastward, eventually reaching the Japanese archipelago via the Zhoushan region of Zhejiang Province^[25,80,81]. This migration pathway showed remarkable congruence with the endemic distribution patterns observed in the biodiversity hotspot regions of eastern China and southern Japan.

Quaternary refugia and land bridge-mediated gene flow

It has been proposed that the continental shelf of the ECS reemerged as a corridor for species migration during the LGM^[18]. Recently, phylogeographic studies on two Sino-Japanese disjunct

species (*Neolitsea sericea* and *Machilus thunbergii*) found genetic signals of lineage admixture on either side of the ECS^[27,82]. One of the most significant discoveries of this study was the detection of two admixed genetic groups coexisting in the populations from Zhoushan, Kyushu, and southwestern Honshu. This pattern provides strong evidence that the ECS land bridge facilitated secondary contact between these groups during the glacial periods. Meanwhile, the minimal differentiation between the Japanese and Korean populations indicated substantial historical gene flow (Supplementary Table S15).

Ecological niche modeling and palynological records demonstrated that *Q. gilva* responded to climatic cooling during the LGM through southward migration, with southern Japan and Jeju Island serving as key refugia^[83,84]. The 'Sino-Japanese admixed' genetic characteristics of Korean populations, combined with geological evidence of the Tsushima land bridge during glacial periods, suggest their postglacial recolonization of the Korean Peninsula from Japanese refugia^[85,86]. Meanwhile, the land bridge across the Taiwan Strait, formed during glacial periods due to lowered sea levels, provided migration corridors for multiple species from mainland China to Taiwan^[19,87–90]. Recurring land connections during the Quaternary glacial–interglacial cycles maintained the gene flow of populations on the mainland and in Taiwan. Notably, based on molecular evidence, we found that the Taiwanese *Q. gilva* population (TCZ) exhibited a complex genetic structure—its genetic

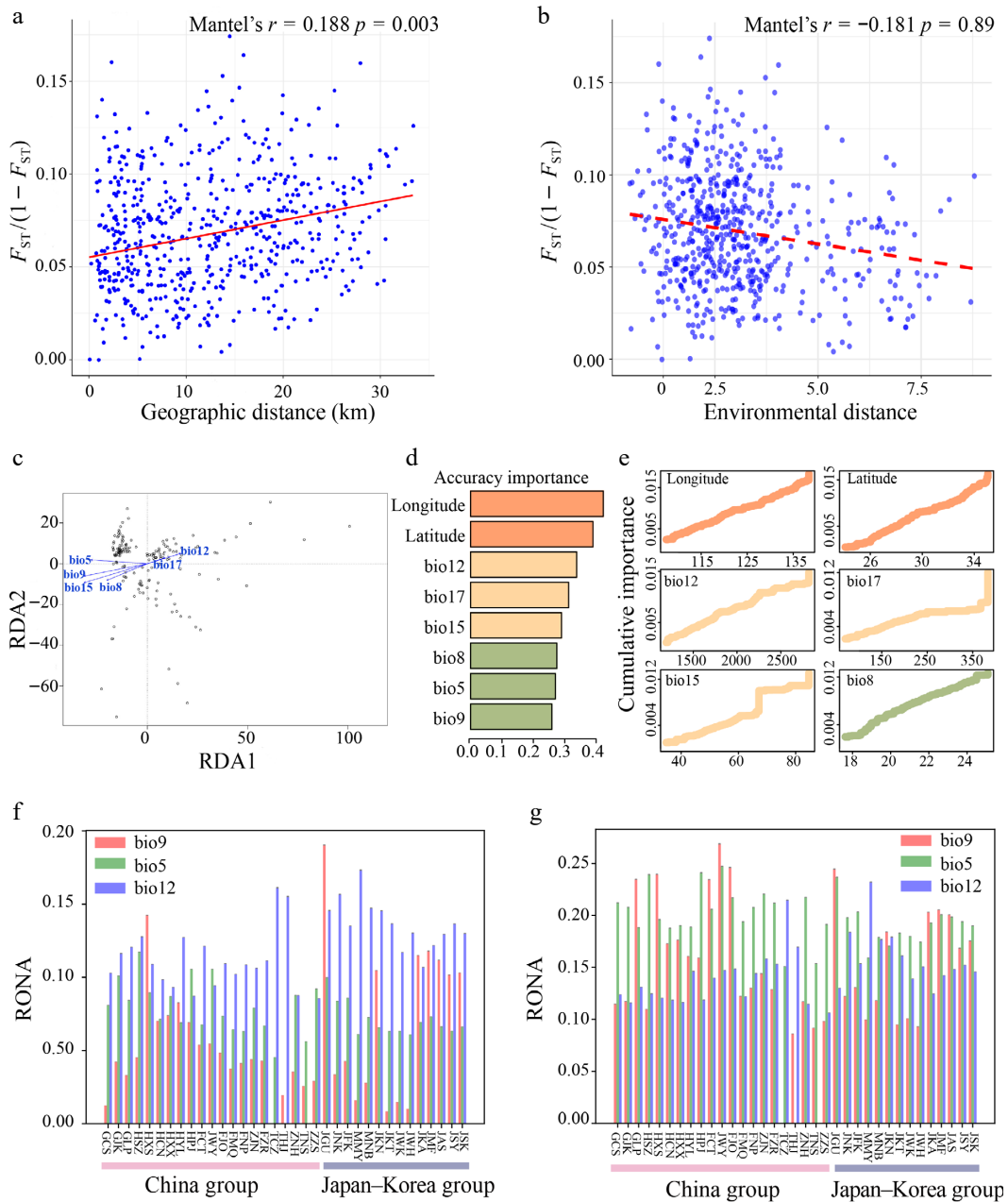


Fig. 5 (a) Mantel test of genetic distance [$F_{ST}/(1 - F_{ST})$] vs. geographical distance. (b) Mantel test of genetic distance [$F_{ST}/(1 - F_{ST})$] vs. environmental distance. (c) Redundancy Analysis (RDA) of *Q. gilva* (Note that the vector length represents the contribution of each environmental variable to the explained variance, while the angles between arrows indicate correlations among variables). (d) Ranked environmental variable importance plot for *Q. gilva* based on Gradient Forest (GF) analysis. (e) I-spline curves illustrating genetic composition variation along environmental gradients. (f) Key environmental factors influencing *Q. gilva* vulnerability under SSP126 (2081–2100). (g) Key environmental factors influencing *Q. gilva* vulnerability under SSP585 (2081–2100).

composition represented an admixture of mainland Chinese and Japanese–Korean groups. Similar biogeographic patterns have been documented in multiple East Asian woody plant taxa (e.g., *Quercus* and *Camphora*)^[91,92], providing compelling evidence for the pivotal role of glacial land bridges in shaping regional biogeographic patterns. The phylogenetic affinities and biogeographic connections of flora among Taiwan of China, mainland of China, and Japan may have been established via multiple pathways: (1) land-bridge connections via the exposed ECS continental shelf during glacial periods; (2) stepping-stone dispersal through the Ryukyu Archipelago; and (3) anthropogenic introductions^[76,93–95].

The phylogeographic history of *Q. gilva* reconstructed in the present study provides a clear example for species evolution of East Asia subtropical EBLFs. Combining this and other studies demonstrates that the contemporary distribution patterns of EBLFs are the products of intertwined long-term natural evolutionary processes (climatic fluctuations and geological events) and recent anthropogenic influences^[77,96–98]. This integrated perspective not only enhances our understanding of how organisms respond to past environmental changes, but also provides a critical framework for predicting and managing their responses to ongoing and future climate change.

Table 1. Effects of environmental and geographical factors on genetic variation decomposed using partial redundancy analysis (pRDA).

Partial RDA models	r^2	Adjusted r^2	p Value
Combined fractions			
Full model: F~env. + F~geog.	0.0628	0.0165	0.001
F~geog.	0.0195	0.0078	0.001
F~env.	0.0473	0.0124	0.001
Individual fractions			
F~geog. env.	0.0155	0.0041	0.001
F~env. geog.	0.0433	0.0087	0.001
Total explained	0.0628		
Total confounded	0.004		
Total unexplained	0.9372		
Total	1		

Evolutionary trajectory and demographic history shaped the genetic diversity of *Q. gilva*

Genetic diversity underpins species' adaptation to environmental changes and their long-term evolutionary potential, and is therefore recognized as a central objective of biodiversity conservation^[99,100]. Although *Q. gilva* is currently assessed as endangered^[32], its genome-wide nucleotide diversity ($\pi \approx 1.4 \times 10^{-2}$) unexpectedly exceeds that of its widespread congeners, including

Q. acutissima, *Q. variabilis*, and *Q. dentata* ($\pi = 0.87 - 0.95 \times 10^{-2}$)^[101,102]. Long-lived organisms such as trees exhibit remarkable resilience in their effective population size over millions of years of glacial cycles, buffering genetic diversity against climatic fluctuations^[103,104]. Our demographic reconstructions support the view that *Q. gilva* has experienced no severe genetic bottlenecks throughout its long evolutionary history, which likely explains its relatively high genetic diversity. In contrast to species that suffer from strong historical bottlenecks^[105], populations of *Q. gilva* may have survived glacial periods in multiple microrefugia, maintaining allelic diversity through postglacial secondary contact^[106]. Furthermore, our RONA analysis (consistently below 0.25) indicated a low mismatch between the genetic composition and future environments, suggesting a robust adaptive capacity. Notably, adaptive introgression is widespread in the genus *Quercus*, and interspecific gene flow may have also contributed to the maintenance of its genetic diversity^[101,107]. Thus, the genetic diversity pattern of *Q. gilva* may benefit from the interplay between its long evolutionary history and complex population dynamics. However, the stark contrast between its high evolutionary potential and its current endangered status underscores the profound impact of recent anthropogenic activities. Deforestation and habitat destruction have caused rapid local population extinctions and severe fragmentation

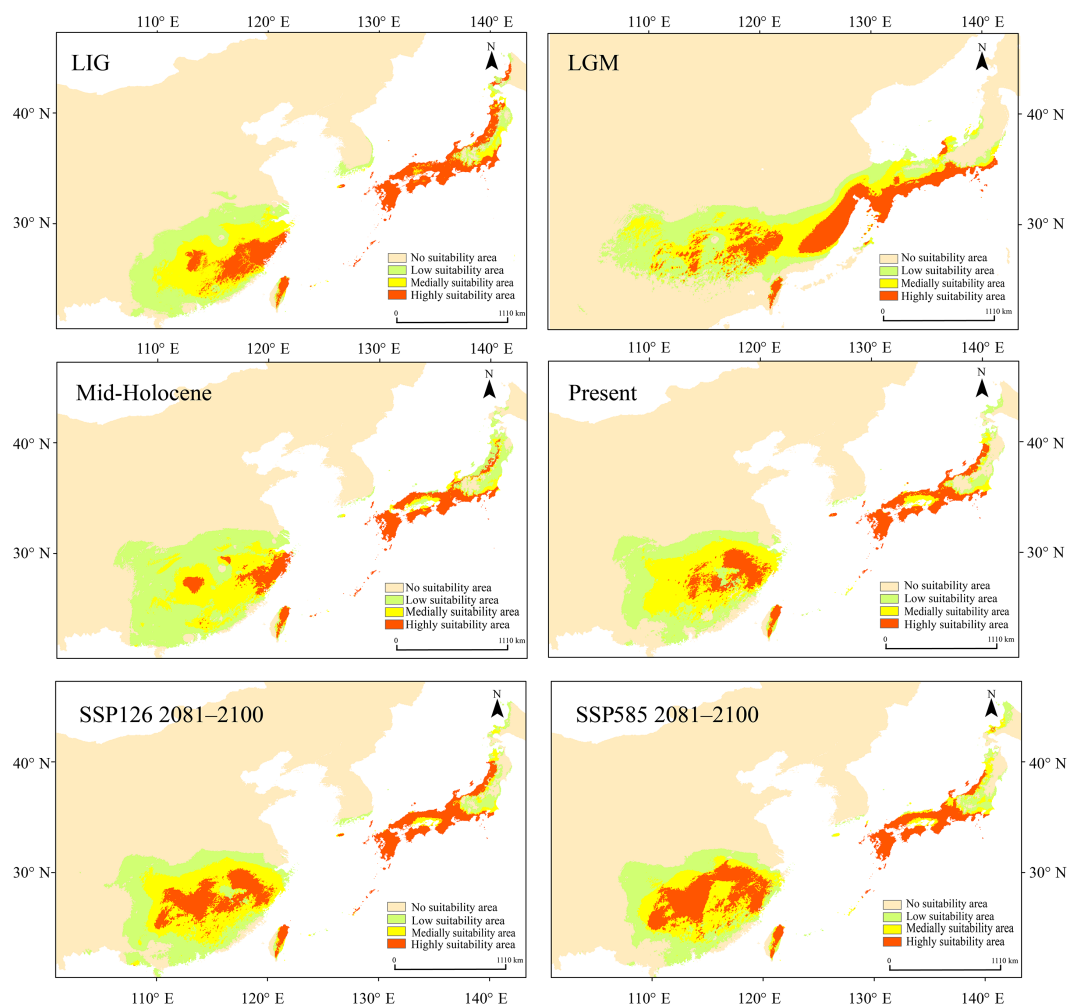


Fig. 6 Maxent was used to simulate the ecological niches of *Q. gilva* over six time periods: Last Interglacial (LIG), Last Glacial Maximum (LGM), Mid-Holocene, present, SSP126 2081–2100, and SSP585 2081–2100. Note that the color gradient from light orange to red in the potential distribution areas represents habitat suitability levels for *Q. gilva*, ranging from unsuitable to optimal conditions.

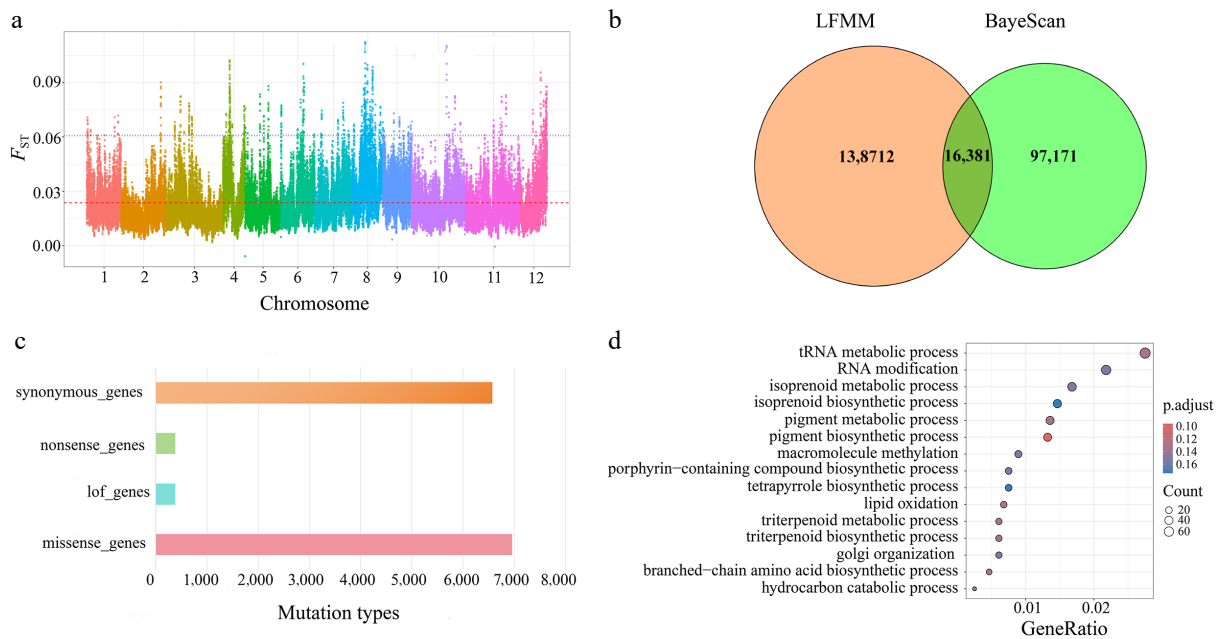


Fig. 7 (a) Highly polymorphic loci for assessing genetic differentiation. (b) Illustrates a Venn diagram showing the detection of outlier loci based on BayeScan and LFMM. (c) Functional annotation performed using snpEff. (d) The results of GO enrichment analysis for missense mutations.

of extant populations^[32]. Thus, this study indicates that although long-term evolutionary history has endowed species with a profound adaptive capacity, short-term, high-intensity anthropogenic disturbances can still rapidly drive them toward extinction^[108].

The subtle but consistent intraspecific difference, where the China group retains slightly higher diversity than the Japan–Korea group (Fig. 2a, Supplementary Table S3), further illuminates our understanding of its biogeographic history. This implies that despite the overarching pattern of high diversity, the complex topography of mainland China (e.g., the interconnected mountain ranges of the Yunnan–Guizhou Plateau and the Wuyi Mountains) may have provided a more stable and connected glacial refugia, better preserving genetic variation^[32]. In contrast, the insular and peninsular nature of the Japan–Korea range likely imposed a greater isolation and bottleneck effect^[32,109,110].

Overall, the genetic structure of *Q. gilva* revealed a significant genetic affinity between the China and Japan–Korea groups of *Q. gilva*. This close genetic connection across geographically isolated populations may provide an evolutionary explanation for the species' biogeographic distribution pattern. Further analyses demonstrated that the complex genetic diversity patterns in *Q. gilva* essentially reflect the dynamic interactions between geological changes and ecological processes, which collectively shape the diversified distribution and adaptive capacity of the species across East Asian landscapes.

Genetic variation of *Q. gilva* in response to environmental gradients and its climate adaptation potential

Under climate change scenarios, understanding the genetic basis of species' adaptation and evaluating their potential to respond to future climates is critical^[111]. Previous studies have employed diverse strategies to reveal the survival risks faced by species under climate change^[112,113]. Mantel tests revealed a significant correlation between genetic differentiation and geographic distance in *Q. gilva* populations. This pattern reflects the species' limited dispersal

capacity: as a wind-pollinated species producing single-seeded nuts with hard pericarps, which are primarily dispersed by small rodents (e.g., squirrels and jays) through scatter-hoarding behavior^[114], and with prolonged germination periods and low germination rates^[115,116], *Q. gilva* exhibits stronger gene flow among neighboring populations and limited exchange between distant ones. Landscape genomic analyses demonstrated that both precipitation and temperature drive adaptive genetic variation in *Q. gilva*, with precipitation exerting a significantly stronger selective pressure than temperature (Fig. 5c–e). Notably, the relative importance of these climatic pressures exhibits distinct regional differentiation among *Quercus* species: genome-wide association studies have identified adaptive SNPs in European populations of *Q. pubescens* and *Q. robur*, primarily associated with precipitation^[117], whereas North American populations of *Q. petraea* and *Q. lobata* showed stronger genetic responses to temperature gradients^[118]. These interspecific differences likely reflect the adaptive divergence strategies of *Quercus* species in response to distinct regional climates^[119]. As a pivotal tectonic driver, the uplift of the Tibetan Plateau since the Miocene dramatically intensified the East Asian monsoon system^[19,80,106], thereby shaping unique hydrothermal regimes across East Asia. This geohistorical process provides a critical environmental context for understanding the stronger adaptive response to precipitation observed in East Asian endemic species such as *Q. gilva*.

Despite this historical adaptive legacy, our study reveals a critical conservation dilemma. Ecological niche modeling projects an expansion of climatically suitable habitats for *Q. gilva* across East Asia, especially in montane- and monsoon-affected regions^[15]. However, this optimistic projection is challenged by the high genomic vulnerability observed in the Japan–Korea group (Supplementary Table S10), indicating a constrained capacity to adapt to climate change. Consequently, even in future suitable habitats, these rear-edge populations may face elevated extinction risks, resulting from a mismatch between environmental opportunities and evolutionary potential^[12].

The molecular evidence strongly supports the environmental adaptation hypothesis of *Q. gilva*. Genome-wide analyses have

revealed significant enrichment of multiple stress-resistance-related functional modules^[120–122]. Regarding ion homeostasis regulation, the enrichment of potassium channels (e.g., *AKT1*) and calcium signaling pathways (GO:0022890) demonstrates their close association with plant salt tolerance, which enhances stress resistance through regulation of the SOS pathway^[123,124]. In the stress response regulatory network, the WRKY transcription factor family (GO:0045893) and SnRK2 protein kinases (GO:0043687) serve as key regulators that improve drought resistance by modulating antioxidant gene expression and participating in ABA signaling pathways, respectively^[125,126]. In terms of metabolic adaptation, sugar metabolism pathways (GO:1901137) and trehalose biosynthesis enhance the adaptive capacity by accumulating osmoregulatory substances and providing thermotolerance protection^[127–129]. These findings are highly consistent with recent studies on adaptive evolution in woody plants^[130,131] and support the 'gene network reprogramming' hypothesis^[132], indicating that *Q. gilva* achieves environmental adaptation through multi-layered regulatory mechanisms. Future research should validate the functions of key genes (e.g., trehalase-6-phosphate synthase) and their specific roles in stress resistance^[133,134].

Therefore, by evaluating how environmental heterogeneity shapes adaptive variation in *Q. gilva* and reveals its genomic vulnerability, we have addressed the second major focus of this study. Our findings not only highlight species-specific adaptation to the East Asian monsoon, but also caution against over-optimistic projections based solely on habitat suitability^[135].

Conclusions

This study establishes, for the first time, an evolutionary history and environmental adaptation framework for the East Asian evergreen broad-leaved tree species *Q. gilva*. Our findings reveal that its biogeographic expansion was jointly driven by the intensification of the Miocene monsoon and the dynamic emergence of land bridges during glacial-interglacial cycles, resulting in divergence between the China and Japan–Korea groups and their subsequent periodic secondary contact with hybrid distribution patterns. We identified annual precipitation as the dominant climatic factor determining its distribution pattern, highlighting species-specific adaptations to precipitation variability in the East Asian monsoon region. These findings not only elucidate the genetic resilience mechanisms of widespread East Asian evergreen broad-leaved tree species during geological and climatic upheavals, but also provide a theoretical baseline for predicting their responses to future climate change. The multidisciplinary integration paradigm proposed in this study offers an universal template for analyzing the eco-evolutionary dynamics of other widely distributed species in monsoon regions.

Author contributions

The authors confirm their contributions to the paper as follows: study conception and design: Song YG, Wang TR, Xu J, Lee JH; data collection: Wang TR, Zheng SS, Yang LH, Li Y, Zhong X, Li XC, Ge BJ, Lu ZJ, Kang YX, Yuan Q, Jin DM, Ning X, Jang YJ, Lee JH, Song YG; analysis and interpretation of results: Wang SS, Wang TR, Wang LL, Huang PH, Liang SD; draft manuscript preparation: Wang SS, Wang TR, Meng HH, Kozłowski G, Xu J, Lee JH, Song YG. All authors reviewed the results and approved the final version of the manuscript.

Data availability

All data have been deposited at the Genome Sequence Archive at the National Genomics Data Center, China National Center for Bioinformation, under accession number CRA028865.

Acknowledgments

This work was supported by the Special Fund for Scientific Research of Shanghai Landscaping & City Appearance Administrative Bureau (Grant Nos G252408 and G192422), the Science and Technology Development Center of National Forestry and Grassland Administration (KJZXSA202214), and the Special Fund for Scientific Research of National Botanical Gardens to benefit sustainable development (the year 2026).

Conflict of interest

The authors declare that they have no conflict of interest.

Supplementary Information accompanies this paper online at: <https://doi.org/10.48130/forres-0026-0016>.

Dates

Received 1 September 2025; Revised 12 March 2026; Accepted 27 March 2026; Published online 28 April 2026

References

- [1] Pina-Martins F, Baptista J, Pappas G Jr, Paulo OS. 2019. New insights into adaptation and population structure of cork oak using genotyping by sequencing. *Global Change Biology* 25:337–350
- [2] Scheffers BR, De Meester L, Bridge TCL, Hoffmann AA, Pandolfi JM, et al. 2016. The broad footprint of climate change from genes to biomes to people. *Science* 354:aaf7671
- [3] Song Y, Meng H, Huang X, Wang A. 2025. Genetic diversity: an important foundation for maintaining biodiversity and a core task of biodiversity conservation. *Biodiversity Science* 33:25383
- [4] Aitken SN, Yeaman S, Holliday JA, Wang T, Curtis-McLane S. 2008. Adaptation, migration or extirpation: climate change outcomes for tree populations. *Evolutionary Applications* 1:95–111
- [5] Sang Y, Long Z, Dan X, Feng J, Shi T, et al. 2022. Genomic insights into local adaptation and future climate-induced vulnerability of a keystone forest tree in East Asia. *Nature Communications* 13:6541
- [6] Dauphin B, Rellstab C, Wüest RO, Karger DN, Holderegger R, et al. 2023. Re-thinking the environment in landscape genomics. *Trends in Ecology & Evolution* 38:261–274
- [7] Capblancq T, Fitzpatrick MC, Bay RA, Exposito-Alonso M, Keller SR. 2020. Genomic prediction of (mal)adaptation across current and future climatic landscapes. *Annual Review of Ecology, Evolution, and Systematics* 51:245–269
- [8] Luqman H, Wegmann D, Fior S, Widmer A. 2023. Climate-induced range shifts drive adaptive response via spatio-temporal sieving of alleles. *Nature Communications* 14:1080
- [9] Zhao W, Sun YQ, Pan J, Sullivan AR, Arnold ML, et al. 2020. Effects of landscapes and range expansion on population structure and local adaptation. *New Phytologist* 228:330–343
- [10] Jia KH, Zhao W, Maier PA, Hu XG, Jin Y, et al. 2020. Landscape genomics predicts climate change-related genetic offset for the widespread *Platycladus orientalis* (Cupressaceae). *Evolutionary Applications* 13:665–676
- [11] Zhu XL, Wang J, Chen HF, Kang M. 2024. Lineage differentiation and genomic vulnerability in a relict tree from subtropical forests. *Evolutionary Applications* 17:e70033

- [12] Wang TR, Meng HH, Wang N, Zheng SS, Jiang Y, et al. 2023. Adaptive divergence and genetic vulnerability of relict species under climate change: a case study of *Pterocarya macroptera*. *Annals of Botany* 132:241–254
- [13] Hewitt G. 2000. The genetic legacy of the Quaternary ice ages. *Nature* 405:907–913
- [14] Ehlers J, Gibbard PL. 2007. The extent and chronology of Cenozoic global glaciation. *Quaternary International* 164–165:6–20
- [15] Tang CQ, Matsui T, Ohashi H, Dong YF, Momohara A, et al. 2018. Identifying long-term stable refugia for relict plant species in East Asia. *Nature Communications* 9:4488
- [16] Zhao J, Li S, Huang J, Ding W, Wu M, et al. 2025. Heterogeneous occurrence of evergreen broad-leaved forests in East Asia: evidence from plant fossils. *Plant Diversity* 47:1–12
- [17] Meng HH, Song YG, Hu GX, Huang PH, Li M, et al. 2025. Evolution of East Asian subtropical evergreen broad-leaved forests: when and how? *Journal of Systematics and Evolution* 63:1045–1060
- [18] Qian H, Ricklefs RE. 2000. Large-scale processes and the Asian bias in species diversity of temperate plants. *Nature* 407:180–182
- [19] Qiu YX, Lu QX, Zhang YH, Cao YN. 2017. 东亚第三纪孑遗植物的亲缘地理学: 现状与趋势 [Phylogeography of East Asia's Tertiary relict plants: current progress and future prospects]. *生物多样性 [Biodiversity Science]* 25:136–146 (in Chinese)
- [20] Naciri Y, Christe C, Bétrisey S, Song YG, Deng M, et al. 2019. Species delimitation in the East Asian species of the relict tree genus *Zelkova* (Ulmaceae): a complex history of diversification and admixture among species. *Molecular Phylogenetics and Evolution* 134:172–185
- [21] Qin SY, Zuo ZY, Guo C, Du XY, Liu SY, et al. 2023. Phylogenomic insights into the origin and evolutionary history of evergreen broadleaved forests in East Asia under Cenozoic climate change. *Molecular Ecology* 32:2850–2868
- [22] Feng L, Wang CY, Zhou LP, Wang YH, Wang J, et al. 2025. Harnessing landscape genomics to evaluate genomic vulnerability and future climate resilience in an East Asia perennial. *Molecular Ecology* 34:e70128
- [23] Cao YN, Zhu SS, Chen J, Comes HP, Wang LJ, et al. 2020. Genomic insights into historical population dynamics, local adaptation, and climate change vulnerability of the East Asian Tertiary relict *Euptelea* (Eupteleaceae). *Evolutionary Applications* 13:2038–2055
- [24] Zhu S, Chen J, Zhao J, Comes HP, Li P, et al. 2020. Genomic insights on the contribution of balancing selection and local adaptation to the long-term survival of a widespread living fossil tree, *Cercidiphyllum japonicum*. *New Phytologist* 228:1674–1689
- [25] Yang LQ, Hu HY, Xie C, Lai SP, Yang M, et al. 2017. Molecular phylogeny, biogeography and ecological niche modelling of *Cardiocrinum* (Liliaceae): insights into the evolutionary history of endemic genera distributed across the Sino-Japanese floristic region. *Annals of Botany* 119:59–72
- [26] Qiu YX, Sun Y, Zhang XP, Lee J, Fu CX, et al. 2009. Molecular phylogeography of East Asian *Kirengeshoma* (Hydrangeaceae) in relation to Quaternary climate change and landbridge configurations. *New Phytologist* 183:480–495
- [27] Jiang K, Tong X, Ding YQ, Wang ZW, Miao LY, et al. 2021. Shifting roles of the East China Sea in the phylogeography of red nanmu in East Asia. *Journal of Biogeography* 48:2486–2501
- [28] Xu WQ, Comes HP, Feng Y, Zhang YH, Qiu YX. 2021. A test of the centre-periphery hypothesis using population genetics in an East Asian Tertiary relict tree. *Journal of Biogeography* 48:2853–2864
- [29] Bai WN, Wang WT, Zhang DY. 2016. Phylogeographic breaks within Asian butternuts indicate the existence of a phylogeographic divide in East Asia. *New Phytologist* 209:1757–1772
- [30] Li M, Wu JJ, Su RP, Fang OY, Cai X, et al. 2025. Genome analyses provide insights into *Engelhardia*'s adaptation to East Asia summer monsoon. *Plant Diversity* 47:718–732
- [31] Ren Y, Zhang L, Yang X, Lin H, Sang Y, et al. 2024. Cryptic divergences and repeated hybridizations within the endangered "living fossil" dove tree (*Davidia involucreata*) revealed by whole-genome resequencing. *Plant Diversity* 46:169–180
- [32] Song YG, Wang TR, Lu ZJ, Ge BJ, Zhong X, et al. 2023. Population survey combined with genomic-wide genetic variation unravels the endangered status of *Quercus gilva*. *Diversity* 15:230
- [33] Han EK, Cho WB, Park JS, Choi IS, Kwak M, et al. 2020. A disjunctive marginal edge of evergreen broad-leaved oak (*Quercus gilva*) in East Asia: the high genetic distinctiveness and unusual diversity of Jeju Island populations and insight into a massive, independent post-glacial colonization. *Genes* 11:1114
- [34] Sugiura N, Tang D, Kurokuchi H, Saito Y, Ide Y. 2015. Genetic structure of *Quercus gilva* Blume in Japan as revealed by chloroplast DNA sequences. *Botany* 93:873–880
- [35] Wang TR, Ning X, Zheng SS, Li Y, Lu ZJ, et al. 2025. Genomic insights into ecological adaptation of oaks revealed by phylogenomic analysis of multiple species. *Plant Diversity* 47:53–67
- [36] Doyle JJ, Doyle JL. 1987. A rapid DNA isolation procedure for small quantities of fresh leaf tissue. *Phytochemical Bulletin* 19:11–15
- [37] Ma Y, Liu D, Wariss HM, Zhang R, Tao L, et al. 2022. Demographic history and identification of threats revealed by population genomic analysis provide insights into conservation for an endangered maple. *Molecular Ecology* 31:767–779
- [38] Chen S, Zhou Y, Chen Y, Gu J. 2018. fastp: an ultra-fast all-in-one FASTQ preprocessor. *Bioinformatics* 34:i884–i890
- [39] Li H, Durbin R. 2009. Fast and accurate short read alignment with Burrows-Wheeler transform. *Bioinformatics* 25:1754–1760
- [40] Li H, Handsaker B, Wysoker A, Fennell T, Ruan J, et al. 2009. The sequence alignment/map format and SAMtools. *Bioinformatics* 25:2078–2079
- [41] Danecek P, Auton A, Abecasis G, Albers CA, Banks E, et al. 2011. The variant call format and VCFtools. *Bioinformatics* 27:2156–2158
- [42] Fu R, Zhu Y, Liu Y, Feng Y, Lu RS, et al. 2022. Genome-wide analyses of introgression between two sympatric Asian oak species. *Nature Ecology & Evolution* 6:924–935
- [43] Chang CC, Chow CC, Tellier LC, Vattikuti S, Purcell SM, et al. 2015. Second-generation PLINK: rising to the challenge of larger and richer datasets. *GigaScience* 4:s13742-015-0047-8
- [44] Yang Z, Ma W, Wang L, Yang X, Zhao T, et al. 2023. Population genomics reveals demographic history and selection signatures of hazelnut (*Corylus*). *Horticulture Research* 10:uhad065
- [45] Alexander DH, Novembre J, Lange K. 2009. Fast model-based estimation of ancestry in unrelated individuals. *Genome Research* 19:1655–1664
- [46] Purcell S, Neale B, Todd-Brown K, Thomas L, Ferreira MAR, et al. 2007. PLINK: a tool set for whole-genome association and population-based linkage analyses. *The American Journal of Human Genetics* 81:559–575
- [47] Wu Q, Dong S, Zhao Y, Yang L, Qi X, et al. 2023. Genetic diversity, population genetic structure and gene flow in the rare and endangered wild plant *Cypripedium macranthos* revealed by genotyping-by-sequencing. *BMC Plant Biology* 23:254
- [48] Lê S, Josse J, Husson F. 2008. FactoMineR: an R package for multivariate analysis. *Journal of Statistical Software* 25:1–18
- [49] Kassambara A, Mundt F. 2020. *Factoextra: extract and visualize the results of multivariate data analyses*. R package version 1.0.7. <https://CRAN.R-project.org/package=factoextra>
- [50] Wickham H. 2016. *ggplot2: elegant graphics for data analysis*. Cham: Springer International Publishing. 260 pp. doi: 10.1007/978-3-319-24277-4
- [51] Nguyen LT, Schmidt HA, von Haeseler A, Minh BQ. 2015. IQ-TREE: a fast and effective stochastic algorithm for estimating maximum-likelihood phylogenies. *Molecular Biology and Evolution* 32:268–274

- [52] Kalyaanamoorthy S, Minh BQ, Wong TKF, von Haeseler A, Jermini LS. 2017. ModelFinder: fast model selection for accurate phylogenetic estimates. *Nature Methods* 14:587–589
- [53] Feng Y, Comes HP, Chen J, Zhu S, Lu R, et al. 2024. Genome sequences and population genomics provide insights into the demographic history, inbreeding, and mutation load of two 'living fossil' tree species of *Dipteronia*. *The Plant Journal* 117:177–192
- [54] Hipp AL, Manos PS, Hahn M, Avishai M, Bodénès C, et al. 2020. Genomic landscape of the global oak phylogeny. *New Phytologist* 226:1198–1212
- [55] Deng M, Jiang XL, Hipp AL, Manos PS, Hahn M. 2018. Phylogeny and biogeography of East Asian evergreen oaks (*Quercus* section *Cyclobalanopsis*; Fagaceae): insights into the Cenozoic history of evergreen broad-leaved forests in subtropical Asia. *Molecular Phylogenetics and Evolution* 119:170–181
- [56] Korunes KL, Samuk K. 2021. Paxy: unbiased estimation of nucleotide diversity and divergence in the presence of missing data. *Molecular Ecology Resources* 21:1359–1368
- [57] Zhang C, Dong SS, Xu JY, He WM, Yang TL. 2019. PopLDdecay: a fast and effective tool for linkage disequilibrium decay analysis based on variant call format files. *Bioinformatics* 35:1786–1788
- [58] Terhorst J, Kamm JA, Song YS. 2017. Robust and scalable inference of population history from hundreds of unphased whole genomes. *Nature Genetics* 49:303–309
- [59] Pickrell JK, Pritchard JK. 2012. Inference of population splits and mixtures from genome-wide allele frequency data. *PLoS Genetics* 8:e1002967
- [60] Fitak RR. 2021. *OptM*: estimating the optimal number of migration edges on population trees using *Treemix*. *Biology Methods and Protocols* 6:bpab017
- [61] Malinsky M, Matschiner M, Svardal H. 2021. Dsuite-Fast *D*-statistics and related admixture evidence from VCF files. *Molecular Ecology Resources* 21:584–595
- [62] Diniz-Filho JAF, Soares TN, Lima JS, Dobrovolski R, Landeiro VL, et al. 2013. Mantel test in population genetics. *Genetics and Molecular Biology* 36:475–485
- [63] Cobos ME, Peterson AT, Barve N, Osorio-Olvera L. 2019. kuenm: an R package for detailed development of ecological niche models using Maxent. *PeerJ* 7:e6281
- [64] Liaw A, Wiener M. 2002. Classification and regression by randomForest. *R News* 2:18–22
- [65] Ellis N, Smith SJ, Pitcher CR. 2012. Gradient forests: calculating importance gradients on physical predictors. *Ecology* 93:156–168
- [66] Coop G, Witonsky D, Di Rienzo A, Pritchard JK. 2010. Using environmental correlations to identify loci underlying local adaptation. *Genetics* 185:1411–1423
- [67] Günther T, Coop G. 2013. Robust identification of local adaptation from allele frequencies. *Genetics* 195:205–220
- [68] Caye K, Jumentier B, Lepeule J, François O. 2019. LFMM 2: fast and accurate inference of gene-environment associations in genome-wide studies. *Molecular Biology and Evolution* 36:852–860
- [69] Cingolani P, Platts A, Wang LL, Coon M, Nguyen T, et al. 2012. A program for annotating and predicting the effects of single nucleotide polymorphisms, SnpEff: SNPs in the genome of *Drosophila melanogaster* strain w¹¹¹⁸; iso-2; iso-3. *Fly* 6:80–92
- [70] Fricot E, François O. 2015. LEA: an R package for landscape and ecological association studies. *Methods in Ecology and Evolution* 6:925–929
- [71] Phillips SJ, Anderson RP, Schapire RE. 2006. Maximum entropy modeling of species geographic distributions. *Ecological Modelling* 190:231–259
- [72] Wang X, Duan Y, Jin L, Wang C, Peng M, et al. 2023. 基于优化的最大熵模型预测中国高山栎组植物的历史、现状与未来分布变化 [Predicting historical, current and future distribution changes of *Quercus* sect. *Heterobalanus* in China using an optimized MaxEnt model]. *生态学报 [Acta Ecologica Sinica]* 43:6590–6604 (in Chinese)
- [73] Gougherty AV, Keller SR, Fitzpatrick MC. 2021. Maladaptation, migration and extirpation fuel climate change risk in a forest tree species. *Nature Climate Change* 11:166–171
- [74] Ke XR, Morales-Briones DF, Wang HX, Sun QH, Landis JB, et al. 2022. Nuclear and plastid phylogenomic analyses provide insights into the reticulate evolution, species delimitation, and biogeography of the Sino-Japanese disjunctive *Diabelia* (Caprifoliaceae). *Journal of Systematics and Evolution* 60:1331–1343
- [75] Li SF, Valdes PJ, Farnsworth A, Davies-Barnard T, Su T, et al. 2021. Orographic evolution of northern Tibet shaped vegetation and plant diversity in eastern Asia. *Science Advances* 7:eabc7741
- [76] Lai YJ, Wen J, Zhou ZK, Ge S, Spicer RA, et al. 2025. Uplift history and biological evolution of the Himalaya (I). *Journal of Systematics and Evolution* 63:1–4
- [77] Lu ZJ, Wang TR, Zheng SS, Meng HH, Cao JG, et al. 2024. Phylogeography of *Pterocarya hupehensis* reveals the evolutionary patterns of a Cenozoic relict tree around the Sichuan Basin. *Forestry Research* 4:e008
- [78] Pound MJ, Haywood AM, Salzmann U, Riding JB. 2012. Global vegetation dynamics and latitudinal temperature gradients during the Mid to Late Miocene (15.97–5.33Ma). *Earth-Science Reviews* 112:1–22
- [79] Lin X, Wyrwoll KH, Chen H, Cheng X. 2016. On the timing and forcing mechanism of a mid-Miocene arid climate transition at the NE margins of the Tibetan Plateau: stratigraphic and sedimentologic evidence from the Sikouzi Section. *International Journal of Earth Sciences* 105:1039–1049
- [80] Lyu R, Xiao J, Li M, Luo Y, He J, et al. 2023. Phylogeny and historical biogeography of the East Asian *Clematis* group, sect. *Tubulosae*, inferred from phylogenomic data. *International Journal of Molecular Sciences* 24:3056
- [81] Wang HX, Moore MJ, Barrett RL, Landrein S, Sakaguchi S, et al. 2020. Plastome phylogenomic insights into the Sino-Japanese biogeography of *Diabelia* (Caprifoliaceae). *Journal of Systematics and Evolution* 58:972–987
- [82] Cao YN, Wang IJ, Chen LY, Ding YQ, Liu LX, et al. 2018. Inferring spatial patterns and drivers of population divergence of *Neolitsea sericea* (Lauraceae), based on molecular phylogeography and landscape genomics. *Molecular Phylogenetics and Evolution* 126:162–172
- [83] Lee JH, Lee DH, Choi BH. 2013. Phylogeography and genetic diversity of East Asian *Neolitsea sericea* (Lauraceae) based on variations in chloroplast DNA sequences. *Journal of Plant Research* 126:193–202
- [84] Jin DP, Park JS, Choi BH. 2021. Historical migration and taxonomic entity of Korean endemic shrub *Lespedeza maritima* (Fabaceae) based on microsatellite loci. *AOB Plants* 13:plab009
- [85] Kong GS, Park SC. 2007. Paleoenvironmental changes and depositional history of the Korea (Tsushima) Strait since the LGM. *Journal of Asian Earth Sciences* 29:84–104
- [86] Lee YG, Choi JM, Oertel GF. 2008. Postglacial sea-level change of the Korean southern sea shelf. *Journal of Coastal Research* 4:118–132
- [87] Gao YD, Zhang Y, Gao XF, Zhu, ZM. 2015. Pleistocene glaciations, demographic expansion and subsequent isolation promoted morphological heterogeneity: a phylogeographic study of the alpine *Rosa sericea* complex (Rosaceae). *Scientific Reports* 5:11698
- [88] Gong W, Liu W, Gu L, Kaneko S, Koch MA, et al. 2016. From glacial refugia to wide distribution range: demographic expansion of *Loropetalum chinense* (Hamamelidaceae) in Chinese subtropical evergreen broadleaved forest. *Organisms Diversity & Evolution* 16:23–38
- [89] He J, Gao Z, Su Y, Lin S, Jiang H. 2018. Geographical and temporal origins of terrestrial vertebrate's endemic to Taiwan. *Journal of Biogeography* 45:2458–2470
- [90] Ye JW, Yang ZZ, Tian B. 2023. Tempo-spatial evolution of seed plant endemism in Taiwan island. *Journal of Biogeography* 50:1981–1991
- [91] Shi MM, Michalski SG, Welk E, Chen XY, Durka W. 2014. Phylogeography of a widespread Asian subtropical tree: genetic east-west differentiation and climate envelope modelling suggest multiple glacial refugia. *Journal of Biogeography* 41:1710–1720

- [92] Jiang XL, Gardner EM, Meng HH, Deng M, Xu GB. 2019. Land bridges in the Pleistocene contributed to flora assembly on the continental islands of South China: insights from the evolutionary history of *Quercus championii*. *Molecular Phylogenetics and Evolution* 132:36–45
- [93] Chiang TY, Schaal BA. 2006. Phylogeography of plants in Taiwan and the Ryukyu Archipelago. *Taxon* 55:31–41
- [94] Chen D, Zhang X, Kang H, Sun X, Yin S, et al. 2012. Phylogeography of *Quercus variabilis* based on chloroplast DNA sequence in East Asia: multiple glacial refugia and mainland-migrated island populations. *PLoS One* 7:e47268
- [95] Kameyama Y, Furumichi J, Li J, Tseng YH. 2017. Natural genetic differentiation and human-mediated gene flow: the spatiotemporal tendency observed in a long-lived *Cinnamomum Camphora* (Lauraceae) tree. *Tree Genetics & Genomes* 13:38
- [96] Qin SY, Zuo ZY, Xu SX, Liu J, Yang FM, et al. 2024. Anthropogenic disturbance driving population decline of a dominant tree in East Asia evergreen broadleaved forests over the last 11, 000 years. *Conservation Biology* 38:e14180
- [97] Xiao S, Li S, Huang J, Wang X, Wu M, et al. 2024. Influence of climate factors on the global dynamic distribution of *Tsuga* (Pinaceae). *Ecological Indicators* 158:111533
- [98] Xu WQ, Ren CQ, Zhang XY, Comes HP, Liu XH, et al. 2024. Genome sequences and population genomics reveal climatic adaptation and genomic divergence between two closely related sweetgum species. *The Plant Journal* 118:1372–1387
- [99] Reed DH, Frankham R. 2003. Correlation between fitness and genetic diversity. *Conservation Biology* 17:230–237
- [100] Hoban S, Bruford MW, da Silva JM, Funk WC, Frankham R, et al. 2023. Genetic diversity goals and targets have improved, but remain insufficient for clear implementation of the post-2020 global biodiversity framework. *Conservation Genetics* 24:181–191
- [101] Shi Y, Zhou BF, Liang YY, Wang B. 2024. Linked selection and recombination rate generate both shared and lineage-specific genomic islands of divergence in two independent *Quercus* species pairs. *Journal of Systematics and Evolution* 62:505–519
- [102] Liang YY, Shi Y, Yuan S, Zhou BF, Chen XY, et al. 2022. Linked selection shapes the landscape of genomic variation in three oak species. *New Phytologist* 233:555–568
- [103] Milesi P, Kastally C, Dauphin B, Cervantes S, Bagnoli F, et al. 2024. Resilience of genetic diversity in forest trees over the Quaternary. *Nature Communications* 15:8538
- [104] Petit RJ, Hampe A. 2006. Some evolutionary consequences of being a tree. *Annual Review of Ecology, Evolution, and Systematics* 37:187–214
- [105] Jaramillo-Correa JP, Bagnoli F, Grivet D, Fady B, Aravanopoulos FA, et al. 2020. Evolutionary rate and genetic load in an emblematic Mediterranean tree following an ancient and prolonged population collapse. *Molecular Ecology* 29:4797–4811
- [106] Qiu YX, Fu CX, Comes HP. 2011. Plant molecular phylogeography in China and adjacent regions: tracing the genetic imprints of Quaternary climate and environmental change in the world's most diverse temperate flora. *Molecular Phylogenetics and Evolution* 59:225–244
- [107] Liu SY, Yang YY, Tian Q, Yang ZY, Li SF, et al. 2025. An integrative framework reveals widespread gene flow during the early radiation of oaks and relatives in Quercoideae (Fagaceae). *Journal of Integrative Plant Biology* 67:1119–1141
- [108] Kardos M, Armstrong EE, Fitzpatrick SW, Hauser S, Hedrick PW, et al. 2021. The crucial role of genome-wide genetic variation in conservation. *Proceedings of the National Academy of Sciences of the United States of America* 118:e2104642118
- [109] Song Y, Xu GB, Long KX, Wang CC, Chen R, et al. 2024. Ensemble species distribution modeling and multilocus phylogeography provide insight into the spatial genetic patterns and distribution dynamics of a keystone forest species, *Quercus glauca*. *BMC Plant Biology* 24:168
- [110] Jiang XL, Deng M, Li Y. 2016. Evolutionary history of subtropical evergreen broad-leaved forest in Yunnan Plateau and adjacent areas: an insight from *Quercus schottkyana* (Fagaceae). *Tree Genetics & Genomes* 12:104
- [111] Fitzpatrick MC, Keller SR. 2015. Ecological genomics meets community-level modelling of biodiversity: mapping the genomic landscape of current and future environmental adaptation. *Ecology Letters* 18:1–16
- [112] Bay RA, Harrigan RJ, Le Underwood V, Gibbs HL, Smith TB, et al. 2018. Genomic signals of selection predict climate-driven population declines in a migratory bird. *Science* 359:83–86
- [113] Butler JB, Harrison PA, Vaillancourt RE, Steane DA, Tibbits JFG, et al. 2022. Climate adaptation, drought susceptibility, and genomic-informed predictions of future climate refugia for the Australian forest tree *Eucalyptus globulus*. *Forests* 13:575
- [114] Xiao Z, Zhang Z, Wang Y. 2004. Dispersal and germination of big and small nuts of *Quercus serrata* in a subtropical broad-leaved evergreen forest. *Forest Ecology and Management* 195:141–150
- [115] Jing MQ, Li ZH, Yang MH, Wu LJ, Song Q. 2012. 赤皮青冈种子质量与萌发特性研究 [The study on seed quality and germination characteristics of *Cyclobalanopsis gilva* (Bl.) Oerst]. *中国农业通报 [Chinese Agricultural Science Bulletin]* 28:27–30 (in Chinese)
- [116] Zaynab M, Pan D, Noman A, Fatima M, Abbas S, et al. 2018. Transcriptome approach to address low seed germination in *Cyclobalanopsis gilva* to save forest ecology. *Biochemical Systematics and Ecology* 81:62–69
- [117] Rellstab C, Zoller S, Walthert L, Lesur I, Pluess AR, et al. 2016. Signatures of local adaptation in candidate genes of oaks (*Quercus* spp.) with respect to present and future climatic conditions. *Molecular Ecology* 25:5907–5924
- [118] Gugger PF, Cokus SJ, Sork VL. 2016. Association of transcriptome-wide sequence variation with climate gradients in valley oak (*Quercus lobata*). *Tree Genetics & Genomes* 12:15
- [119] Martins K, Gugger PF, Llanderal-Mendoza J, González-Rodríguez A, Fitz-Gibbon ST, et al. 2018. Landscape genomics provides evidence of climate-associated genetic variation in Mexican populations of *Quercus rugosa*. *Evolutionary Applications* 11:1842–1858
- [120] Guo Z, Yang W, Chang Y, Ma X, Tu H, et al. 2018. Genome-wide association studies of image traits reveal genetic architecture of drought resistance in rice. *Molecular Plant* 11:789–805
- [121] Quan M, Liu X, Du Q, Xiao L, Lu W, et al. 2021. Genome-wide association studies reveal the coordinated regulatory networks underlying photosynthesis and wood formation in *Populus*. *Journal of Experimental Botany* 72:5372–5389
- [122] De La Torre AR, Sekhwal MK, Puiui D, Salzberg SL, Scott AD, et al. 2022. Genome-wide association identifies candidate genes for drought tolerance in coast redwood and giant sequoia. *The Plant Journal* 109:7–22
- [123] Zhao S, Zhang Q, Liu M, Zhou H, Ma C, et al. 2021. Regulation of plant responses to salt stress. *International Journal of Molecular Sciences* 22:4609
- [124] Dong Q, Wallrad L, Almutairi BO, Kudla J. 2022. Ca²⁺ signaling in plant responses to abiotic stresses. *Journal of Integrative Plant Biology* 64:287–300
- [125] Hasan MM, Liu XD, Waseem M, Yao GQ, Alabdallah NM, et al. 2022. ABA activated SnRK2 kinases: an emerging role in plant growth and physiology. *Plant Signaling & Behavior* 17:2071024
- [126] Javed T, Gao SJ. 2023. WRKY transcription factors in plant defense. *Trends in Genetics* 39:787–801
- [127] Carraro E, Di Iorio A. 2022. Eligible strategies of drought response to improve drought resistance in woody crops: a mini-review. *Plant Biotechnology Reports* 16:265–282
- [128] Ren S, Ma K, Lu Z, Chen G, Cui J, et al. 2019. Transcriptomic and metabolomic analysis of the heat-stress response of *Populus tomentosa* Carr. *Forests* 10:383

- [129] Yang J, Zhang J, Li C, Zhang Z, Ma F, et al. 2019. Response of sugar metabolism in apple leaves subjected to short-term drought stress. *Plant Physiology and Biochemistry* 141:164–171
- [130] Kijowska-Oberc J, Staszak AM, Kamiński J, Ratajczak E. 2020. Adaptation of forest trees to rapidly changing climate. *Forests* 11:123
- [131] Miryeganeh M, Armitage DW. 2025. Epigenetic responses of trees to environmental stress in the context of climate change. *Biological Reviews* 100:131–148
- [132] Artur MAS, Kajala K. 2021. Convergent evolution of gene regulatory networks underlying plant adaptations to dry environments. *Plant, Cell & Environment* 44:3211–3222
- [133] Jinek M, Chylinski K, Fonfara I, Hauer M, Doudna JA, et al. 2012. A programmable Dual-RNA-guided DNA endonuclease in adaptive bacterial immunity. *Science* 337:816–821
- [134] Gootenberg JS, Abudayyeh OO, Lee JW, Essletzbichler P, Dy AJ, et al. 2017. Nucleic acid detection with CRISPR-Cas13a/C2c2. *Science* 356:438–442
- [135] Yuan S, Shi Y, Zhou BF, Liang YY, Chen XY, et al. 2023. Genomic vulnerability to climate change in *Quercus acutissima*, a dominant tree species in East Asian deciduous forests. *Molecular Ecology* 32:1639–1655



Copyright: © 2026 by the author(s). Published by Maximum Academic Press, Fayetteville, GA. This article is an open access article distributed under Creative Commons Attribution License (CC BY 4.0), visit <https://creativecommons.org/licenses/by/4.0/>.